Desalination and Water Treatment
www.deswater.com

doi: 10.5004/dwt.2017.20895

80 (2017) 370–379
June

Removal of methyl orange from aqueous solution with crosslinked quaternized chitosan/bentonite composite

Pan Hu†, Lujie Zhang†, Jing Wang, Ruihua Huang*

College of Chemistry and Pharmacy, Northwest A&F University, Yangling, Shaanxi 712100, China, Tel. +86 029 87092226; emails: hrh20022002@163.com (R. Huang), 1515325595@qq.com (P. Hu), 1065849947@qq.com (L. Zhang), 1396543866@qq.com (J. Wang)

Received 30 September 2016; Accepted 10 May 2017

ABSTRACT

A crosslinked quaternized chitosan (*N*-2-hydroxypropyl-trimethylammonium chloride chitosan)/bentonite (CHTCC/BT) composite was developed via immobilizing crosslinked quaternized chitosan into bentonite and characterized by X-ray diffraction and fourier transform infrared spectroscopy techniques. This composite was applied for the adsorption of methyl orange (MO) from aqueous solution. Effects of the amount of quaternized chitosan in the CHTCC/BT composite, initial pH, initial dye concentration, inorganic sodium salt and ionic strength on MO adsorption were studied in detail using a batch method. Increasing the amount of quaternized chitosan in the CHTCC/BT composite enhanced the adsorption of MO while increasing initial pH, initial dye concentration and ionic strength decreased the adsorption of MO. The adsorption kinetics followed the mechanism of the pseudo-second-order equation. The equilibrium data were described by the Langmuir model. The monolayer adsorption capacity of CHTCC/BT composite was 632.9 mg/g at 298 K and natural pH value. The adsorbent was prone to regeneration with 0.3 mol/L NaOH solution. The possible pathways for MO adsorption may include the electrostatic interaction and hydrogen bonding between CHTCC/BT composite and MO.

Keywords: Quaternized chitosan; Adsorption; Bentonite; Isotherms

1. Introduction

Numerous textile or printing industries, which mainly use dyes, release a large amount of highly colored effluents into the environment, probably containing more than 10^5 kinds of commercial dyes and over 7 million tons annually [1]. The discharge of colored effluent even at very low concentrations can have a potentially destructive effect on aquatic systems [2]. Many methods have been employed for the removal of dyes from colored effluents, such as membrane filtration [3], oxidation, coagulation [4], biological treatment, electrochemical process and adsorption [5–7]. Among these techniques, adsorption presents important advantages over the other methods because of simple operation, high treatment efficiency and economy [2]. In recent years, much attention was paid to the search for low-cost adsorbents with pollutant-binding capacities, such as natural materials, agricultural wastes and industrial wastes.

Bentonite (BT), which is mainly composed of montmorillonite, is a layered mineral with a crystalline structure and net negative surface charge. Natural BT exhibited low adsorption capacity for anionic pollutants due to the net negative charge surface. However, BT can be easily modified by cationic exchange reactions between the sodium ions in the montmorillonite layers and cations, such as Ni, Co, Zn, cationic surfactants and polymers [8–10]. However, some cationic substances are difficult to degrade in nature and may be toxic to humans and the environment. Therefore, the use of biodegradable polymers, such as chitosan has generated the increasing attention. A quaternized chitosan, *N*-2-hydroxypropyl-trimethylammonium chloride chitosan

* Corresponding author.

†Both authors contributed equally to this work.

(HTCC), as a cationic polymer, is one of the derivatives from chitosan. It is itself a good adsorbent and flocculent agent due to its unique properties, such as biocompatibility, biodegradation, biological activity, low toxicity, etc. [11]. Li et al. [12] investigated the adsorption of both methyl orange (MO) and chromium from their aqueous solutions using a quaternary ammonium salt modified chitosan magnetic composite adsorbent. The results showed that the quaternary ammonium salt modified chitosan magnetic adsorbent had evidently high adsorption capacities for both anionic pollutants ascribed to the additional quaternary ammonium salt groups as compared with chitosan magnetic adsorbent without modification. At present, though there were lots of studies about clay–chitosan composite for making composite films, sensors, adsorbent material [13], enzyme immobilization supports and nanocomposites [14,15], there are few reports on the preparation or application of quaternized chitosan immobilized BT composite. Luo et al. [16] demonstrated that the modification of montmorillonite with quaternized chitosan could enhance the adsorption capacity of montmorillonite in comparison with quaternized chitosan resin without montmorillonite. In our previous study, it was also found that the HTCC/BT composite showed high adsorption capacity for anionic Cr(VI) [17].

In this study, the crosslinked quaternized chitosan (CHTCC) would be attempted to modify BT. Though the quaternized chitosan (HTCC) is itself a good adsorbent, it is costly. Besides, it was prone to loss due to its water solubility during the application in wastewater treatment, thus, it was often modified. The combining of HTCC with other low-cost materials would result in the decreased cost of adsorbents and the enhanced stability of adsorbents. Meanwhile, it was also expected that the resultant composite could exhibit a high binding capacity for anionic dyes due to the introduction of positively charged quaternary ammonium groups. MO would be chosen as a model dyes in this study because it is a common water-soluble azo dye, which is widely used in chemical, textile and paper industries, and it is seriously hazardous to the environment. The color index number of MO is 13025. This study evaluated the adsorption capacity of CHTCC/BT composite for MO from aqueous solutions. Effects of the amount of HTCC, pH value of MO solution, initial MO concentration and ionic strength on MO adsorption were examined. The equilibrium data were analyzed using Langmuir, Freundlich and Dubinin–Radushkevich (D–R) isotherm models. The kinetic constants of the experimental data were determined using the pseudo-first-order and pseudo-second-order models. Besides, the regeneration of the adsorbent was evaluated.

2. Materials and methods

2.1. Materials

Chitosan was purchased from the Sinopharm Group Chemical Reagent Limited Company (China) with a degree of deacetylation of 90% and average molecular weight of 10^5 g/mol. HTCC, with a substitution degree of 89.3%, was prepared according to our previous literature [14]. The reaction scheme of HTCC is depicted in Fig. 1(a). BT powder with a particle size of 200-mesh was acquired from the chemical

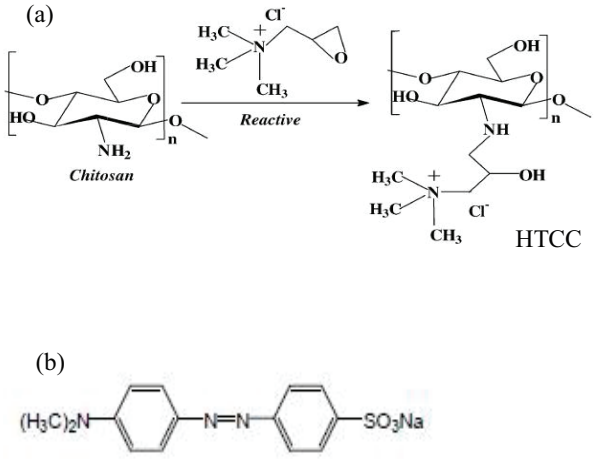

Fig. 1. Reaction scheme of HTCC (a) and molecular structure of MO (b).

factory of Shentai, Xinyang, Henan, China. MO was supplied by Sigma Chemical Company (Shanghai, China), and used as adsorbate in this study. The molecular structure of MO is presented in Fig. 1(b). MO concentrations were measured using a UV–Vis spectrometer at 464 nm. All other reagents were of analytical grade. Initial pH value of MO solutions was adjusted by adding 0.1 mol/L HCl or NaOH solutions.

2.2. Preparation of CHTCC/BT composite

HTCC (1 g) was dissolved in 50 mL of distilled water under constant stirring for 2 h at 25°C. About 1 g of BT was added and then mixed for 5 h. The resulting HTCC–clay solution was uniformly coated in the Petri dishes, and allowed to stay at 60°C in an oven to form membranes. After immersing in a solution of 5% epichlorohydrin in ethanol at 60°C for 20 h, these membranes were washed using distilled water to remove any impurities and dried in an oven at 60°C for 24 h. After drying, the membranes were ground and sieved. The particles of 100-mesh size for the crosslinked HTCC immobilized BT composite were obtained, and used for adsorption studies. The resultant composite was referred to CHTCC/BT composite.

2.3. Characterization of CHTCC/BT composite

FTIR analysis of CHTCC/BT composite was conducted in a FTIR spectrometer (Shimadzu 4100), using the transmittance method with wavelength between 400 and 4,000 cm^{-1} at a resolution of 4 cm^{-1}. X-ray diffraction (XRD) patterns were recorded on a Shimadzu XD3A diffractometer with Cu Kα radiation for the identification of crystalline phase. The samples were recorded from 5° to 55° with a scan rate of 0.02°/s.

The point of zero charge (pH_{pzc}) for the quaternized chitosan immobilized BT was determined according to the method described by the solid addition method [18]. Initial pH of 50 mL of 0.1 mol/L NaCl solutions (pH_i) was adjusted from pH 1 to 10 by adding either 0.1 mol/L HCl or 0.1 mol/L NaOH solutions. CHTCC/BT composite (0.01 g) was added to 50 mL of 0.1 mol/L NaCl solution and was shaken for

60 min. Final pH (pH_f) of the solution was measured. The difference between the initial and final pH ($pH_f - pH_i$) was plotted against the initial pH (pH_i) and the point where $pH_f - pH_i = 0$ was thought to be the point of zero charge (pH_{pzc}) of adsorbent.

2.4. Kinetic experiments

Kinetic experiments were conducted in order to determine the time needed to reach equilibrium and adsorption rates of dye. Adsorption kinetics experiments at different concentrations (100, 200, 300 and 500 mg/L) were carried out by the batch method, where 0.02 g of adsorbent was added to 50 mL MO solutions. The samples were agitated for times varying from 5 to 180 min. At the end of each adsorption period, the samples were collected by filtration, and the concentrations of the residual MO in the filtrates were then determined. The removal, R, and adsorption capacity, q_t (mg/g), at t, were calculated as follows:

$$q_t = (C_0 - C_t) \times \frac{V}{M} \tag{1}$$

$$R = 100 \times \frac{(C_0 - C_t)}{C_0} \tag{2}$$

where C_0 and C_t are the concentrations of MO in the initial solution and at time, t, (mg/L), respectively; V is the volume of MO solution (L) and M is the mass of adsorbent (g).

2.5. Isotherm experiments

The equilibrium study was conducted by agitating 0.02 g of adsorbent in 50 mL MO solutions for 100 min at different temperatures (298, 308, 318 and 328 K). The concentrations of MO solutions changed from 100 to 800 mg/L. After equilibrium, the adsorbent was separated by filtration and the concentrations of the residual MO in the filtrates were then determined. The adsorption capacity, q_e (mg/g), at equilibrium, was calculated as follow:

$$q_e = (C_0 - C_e) \times \frac{V}{M} \tag{3}$$

where C_0 and C_e are the concentrations of MO in the initial solution and at equilibrium (mg/L), respectively; V is the volume of MO solution (L) and M is the mass of adsorbent (g).

2.6. Desorption experiments

In this study, the adsorption experiments were conducted by adding 0.02 g of adsorbents in 50 mL MO solution (100 mg/L) and agitated for 100 min at 298 K. In the desorption process, the adsorbents loaded by MO were added into 50 mL eluents and agitated for 2 h at 298 K. After the regenerated adsorbents were washed with distilled water several times, and dried, they were applied for the adsorption of MO again. In the desorption process, these eluents including NaOH, NaCl and HCl solutions were tested.

3. Results and discussion

3.1. Effect of the amount of HTCC on MO adsorption

To investigate the effect of the amount of HTCC on MO adsorption, the adsorption experiments were performed at 298 K. 0.02 g of adsorbent was added to 50 mL MO solutions (100 and 200 mg/L) and continuously agitated at 200 rpm for 60 min. The results are shown in Fig. 2. Increasing the amount of HTCC enhanced the removal toward MO. This increase may be attributed to the electrostatic interaction between the cationic charges of HTCC and the anionic charges of MO molecules. Higher amounts of HTCC provided more cationic charges and consequently a stronger electrostatic interaction with the anionic dye occurred. Beyond 1.0 g of HTCC, a further increase in the amount of HTCC only showed a slight effect on MO adsorption. Therefore, 1.0 g of HTCC was applied in the preparation of this composite without special description.

3.2. Effect of initial dye concentration

For this test, the adsorption experiments were carried out at 298 K. 0.02 g of adsorbent was added to 50 mL of aqueous MO solutions varying from 100 to 500 mg/L and continuously agitated at 200 rpm for 60 min. As shown in Fig. 3(a), increasing the MO concentrations decreased the MO adsorption onto this composite. In this study, the adsorbent dosage was kept fixed. A fixed adsorbent dosage reflects the constant adsorption sites. As the dye concentration increased, the ratio of adsorption sites to the number of dye molecules would decrease because more adsorption sites were unavailable for the adsorption of dye molecules. Therefore, at higher dye concentrations, lower removal was observed. Similar results have been reported in the literatures [19,20].

3.3. Effect of pH value of MO solutions

The pH value of dye solutions plays an important role in adsorption process. To estimate the effect of pH on MO

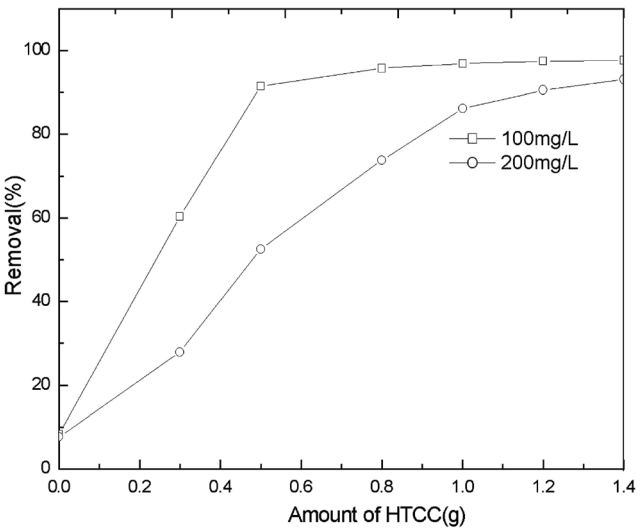

Fig. 2. Effect of the amount of HTCC on MO adsorption.

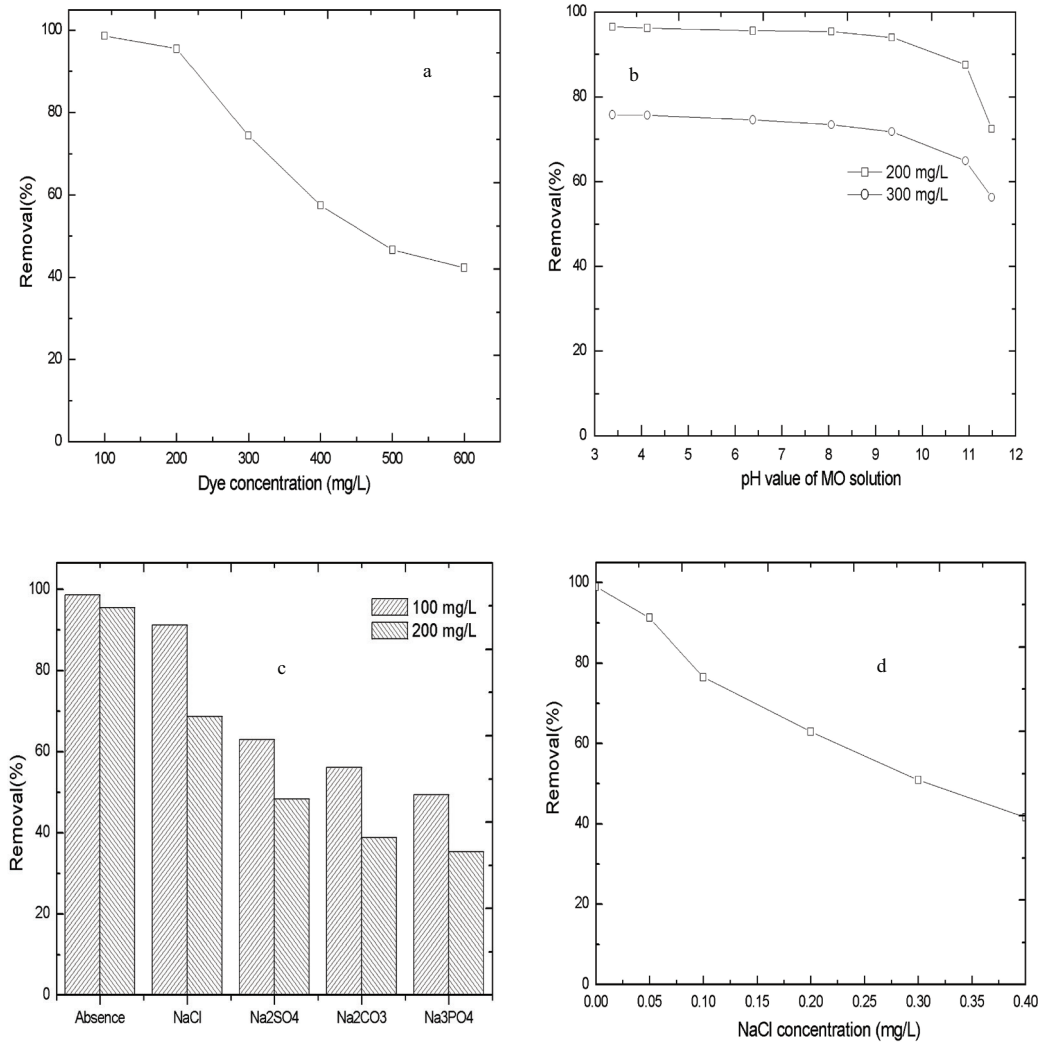

Fig. 3. Effects of MO concentration (a), initial pH value of MO solution (b), inorganic sodium salt (c) and ionic strength (d) on MO adsorption.

adsorption by this composite, the adsorption experiments were conducted at 298 K. 0.02 g of adsorbent was added to 50 mL MO solutions (200 and 300 mg/L) and continuously agitated at 200 rpm for 60 min. The pH value of MO solutions varied from 3 to 11. The results are shown in Fig. 3(b). High removal was observed in a wide pH range of 3–9. The removal was 95.3% and 74.2% for MO solutions with 200 and 300 mg/L at natural pH, respectively. To better understand the effect of initial pH value on adsorption, the plot for the measurement of pH_{pzc} of this adsorbent was presented in Fig. S1 in the supplementary materials and obtained at 7.2 or so. The surface of the adsorbent will be negatively charged above pH_{pzc} and positively charged below pH_{pzc}. The sulfonate groups of MO ($–SO_3Na$) were dissociated and converted to anionic dye ions $–SO_3^-$ in aqueous solution. In acidic media ($<pH_{pzc}$), the surface of this adsorbent was positively charged, which facilitated the electrostatic attractions between the anionic groups $–SO_3^-$ of dyes and the positively charged surface of this composite, thus resulted in an increase in dye adsorption. However, when increasing pH values, the number of the negatively charged sites increased, thus a decrease in removal with increasing pH was attributed to the decreasing the electrostatic attractions. Beyond pH 9, a sharp decline in removal was observed due to the decreased positively charges of the adsorbent as well as the competitive adsorption of the abundant OH^- ions and anionic MO for the adsorption sites.

3.4. Effects of inorganic sodium salt and ionic strength

Sodium salt is often used as a stimulator in dying industries. Effect of inorganic sodium salt (0.05 mol/L) on MO adsorption is presented in Fig. 3(c). The presence of inorganic sodium salts decreased MO adsorption by this composite. This decrease followed the order: $PO_4^{3-} > CO_3^{2-} > SO_4^{2-} > Cl^-$. For SO_4^{2-} and Cl^-, the decreased removal may result from their competitive adsorption with MO for adsorptive sites. For PO_4^{3-} and CO_3^{2-}, the addition of CO_3^{2-} and PO_4^{3-} enhanced the pH values of MO solutions. As presented in the results of pH effect in section 3.3, the removal decreased when the pH value of MO solution increased, especially beyond pH 9. The dramatically

decreased removal in the presence of PO_4^{3-} and CO_3^{2-} may be due to their competitive adsorption as well as the increased pH value. To further understand the effect of inorganic salts on MO adsorption, the concentration of MO solution tested was 100 mg/L and various NaCl concentrations were applied to conduct the adsorption experiments. The results in Fig. 3(d) show that increasing NaCl concentration (ionic strength) weakened the adsorption of MO onto this composite. Previous studies showed that if the electrostatic attraction is the main adsorption mechanism, the ionic strength has a significant negative effect on the adsorption process [21–23]. Thus, our results indicated that the electrostatic interaction between MO and this composite was the main interaction in MO adsorption.

3.5. Kinetic experiments

Kinetic experiments were conducted in order to determine the time needed to reach equilibrium and adsorption rates of dye. Adsorption kinetic experiments at different concentrations (100, 200, 300 and 500 mg/L) were performed by the batch method, where 0.02 g of adsorbent was added to 50 mL MO solution. The samples were agitated for times varying from 5 to 180 min. At the end of each adsorption period, the samples were collected by filtration, and the concentrations of the residual MO in the filtrates were then determined. As shown in Fig. 4, the adsorption of MO onto this adsorbent approached constant values after a period of 100 min, and thus the time required for the adsorption equilibrium was 100 min. The data were modeled using both first- and second-order kinetic models. The pseudo-first-order model can be expressed according to Eq. (4) [24]:

$$\frac{1}{q_t} = \frac{k_1}{q_e t} + \frac{1}{q_e} \tag{4}$$

where q_e (mg/g) and q_t (mg/g) are the amounts of MO adsorbed at equilibrium and at different time intervals, respectively. k_1 (1/min) is the rate constant of pseudo-first-order model. Linear plots of "$\log(1/q_t)$ vs. $1/t$ " were used to predict k_1 and q_e from the slope and intercept, respectively.

The pseudo-second-order model can be expressed according to Eq. (5) [25]:

$$\frac{t}{q_t} = \frac{1}{k_2 q_e^2} + \frac{1}{q_e} t \tag{5}$$

where k_2 (g/mg min) is the rate constant of the pseudo-second-order adsorption process. The values of k_2 and q_e can be determined from the slope and intercept of the "t/q_t vs. t" plots, respectively.

These plots are presented in Fig. S2 in the supplementary materials and the parameters obtained are summarized in Table 1. Though the calculated q_e values from both models agreed very well with the experimental ones, the values for R^2 of pseudo-second-order model were all much closer to 1.0 than those of pseudo-first-order model, indicating that the pseudo-second-order equation was more suitable to describe the adsorption kinetics of CHTCC/BT composite for MO. The similar results were also reported by some authors [26,27].

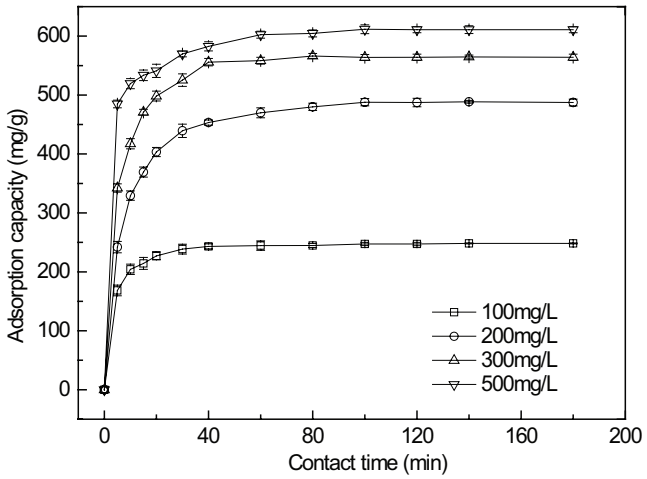

Fig. 4. Plots of the adsorption capacity vs. contact time at different MO concentrations.

3.6. Adsorption isotherm study

Adsorption isotherm models describe the relationship between adsorbates and adsorbents when the adsorption process reaches equilibrium. These equilibrium data of MO onto this composite at different temperatures were fitting to the Langmuir, Freundlich and Dubinin–Radushkevich (D–R) isotherm models. The Langmuir adsorption model assumes that the maximum adsorption corresponds to a saturated

Table 1
Kinetic parameters of the adsorption of MO onto the CHTCC/BT composite

Models	Parameters	Concentration (mg/L)			
		100	200	300	500
Pseudo-first-order	$q_{e,\exp}$ (mg/g)	249.4	497.3	566.7	611.2
	$q_{e,\mathrm{cal}}$ (mg/g)	254.5	512.8	584.8	606.1
	k_1 (1/min)	2.524	5.549	3.614	1.442
	R^2	0.9966	0.9994	0.9953	0.9495
Pseudo-second-order	$q_{e,\mathrm{cal}}$ (mg/g)	250.6	505.1	574.7	617.3
	k_2 (g/mg min)	0.0002	0.0004	0.0006	0.0008
	R^2	0.9999	1.000	1.000	0.9999

monolayer adsorption on the homogeneous surface. The Langmuir equation [28] is expressed as:

$$\frac{C_e}{q_e} = \frac{1}{Qb} + \frac{C_e}{Q} \tag{6}$$

where Q is the maximum amount of adsorption with complete monolayer coverage on the adsorbent surface (mg/g) and b is the Langmuir constant, which is related to the energy of adsorption (L/mg). From the linear plots of C_e/q_e against C_e, Q and b values can be calculated from the slope and intercept, respectively.

The Freundlich isotherm can be applied for non-ideal sorption on heterogeneous surfaces and multilayer sorption. The Freundlich equation [29] is expressed as:

$$\log q_e = \log K_f + \frac{1}{n}\log C_e \tag{7}$$

where K_f [(mg/g)(L/mg)$^{1/n}$] and n are Freundlich constants related to adsorption capacity and heterogeneity factor, respectively. K_f and n values can be calculated from the intercept and slope of the linear plots between logC_e and logq_e.

The D–R isotherm equation, which is more generally used to distinguish between physical and chemical adsorption, is represented by the following equation [30]:

$$\ln q_e = \ln q_m - \beta\varepsilon^2 \tag{8}$$

where q_e is the amount of dye adsorbed (mg/g), X_m is the maximum adsorption capacity of dye (mg/g), β is the D–R constant (kJ^2/mol^2) and ε is the Polanyi potential given by Eq. (9):

$$\varepsilon = RT\ln(1 + 1/C_e) \tag{9}$$

where R is the gas constant in J/mol K, T is the temperature (K) and C_e is the equilibrium concentration of MO (mol/L). The linear plot of lnq_e against ε gives the values of β and X_m from slope and intercept, respectively. The constant β is related to the mean free energy of sorption and this can be computed using the following relationship:

$$E = \frac{1}{\sqrt{2\beta}} \tag{10}$$

where E is the mean adsorption energy (kJ/mol) and β is the D–R constant (kJ^2/mol^2). The E value ranges from 1 to 8 kJ/mol for physical sorption and 8–16 kJ/mol for chemical sorption.

These plots are presented in Fig. S3 in the supplementary materials and the relative parameters of Langmuir, Freundlich and D–R adsorption isotherms are listed in Table 2. The plots for the experimental and calculated data from three isotherm models are depicted in Fig. 5. Based on the R^2 values, the adsorption of MO onto the CHTCC/BT composite was best described by the Langmuir model. This implied the monolayer distribution of MO molecules onto the homogeneous active sites on the adsorbent surface. The maximum monolayer Q was obtained at 632.9 mg/g at 298 K and natural pH. However, increasing temperature decreased the adsorption of MO onto this composite, suggesting that the adsorption of MO was favored at low temperatures and it was an exothermic process. Meanwhile, Fig. 5 shows that the calculated data from Langmuir model were closer to the experimental ones as compared with those from Freundlich and D–R models.

In addition, the E values in all experiments tested were found in the range of 1–8 kJ/mol, indicating that the governing type of adsorption was essentially physical. Therefore, the adsorption of MO from aqueous solution formed a monolayer onto the adsorbent surface generally through physical adsorption.

3.7. Desorption study

To evaluate the reusability of this composite, the regenerated adsorbents were used to adsorb MO again. As presented in Table 3, 0.3 mol/L NaOH and NaCl solutions were effectively applied for the regeneration of this adsorbent. The regenerated adsorbents with 0.3 mol/L NaOH solution still exhibited high removal toward MO, indicating that the adsorption of MO onto this adsorbent was conducted by electrostatic interaction. This result corroborated well the explanation of pH effect investigated in section 3.3. HCl solutions was unable to break this binding in interaction effectively, thus the regeneration using HCl solutions was unsatisfactory.

Table 2
Adsorption isotherm parameters of MO onto the CHTCC/BT composite

Isotherms	Parameter	Temperature (K)			
		298	308	318	328
Langmuir	b (L/mg)	0.1503	0.2080	0.2624	0.4041
	Q (mg/g)	632.9	621.1	591.7	558.7
	R^2	0.9986	0.9973	0.9989	0.9998
Freundlich	K_f[(mg/g)(L/mg)$^{1/n}$]	323.3	317.0	314.4	304.7
	$1/n$	0.1276	0.1251	0.1194	0.1170
	R^2	0.8725	0.9075	0.8958	0.8933
D–R	X_m (mg/g)	570.7	548.4	538.6	511.4
	β (kJ^2/mol^2)	3.27E–7	2.02E–7	2.23E–7	1.82E–7
	E (kJ/mol)	1.2	1.6	1.5	1.7
	R^2	0.9458	0.9304	0.9533	0.9103

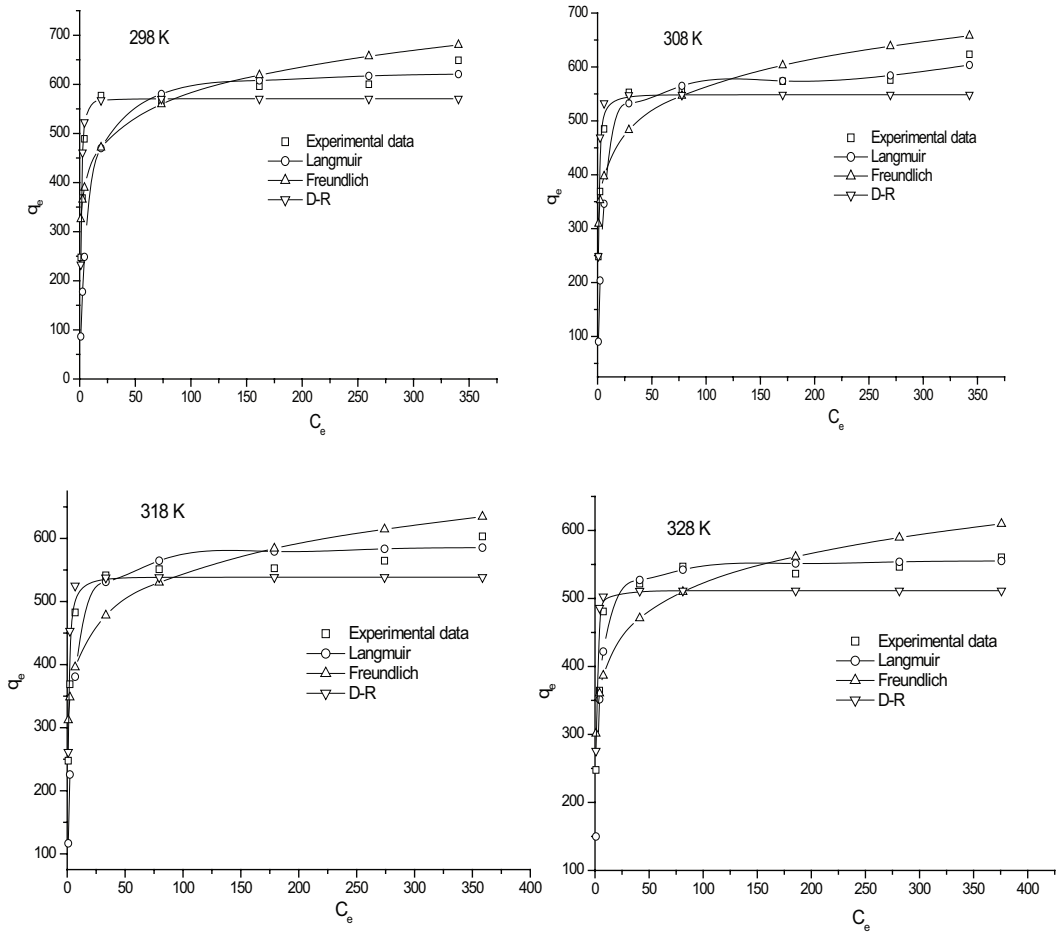

Fig. 5. Plots for the experimental and calculated data from three isotherm models at different temperatures.

Table 3
Regeneration of crosslinked quaternized chitosan/bentonite composite

Types of eluent	Eluent concentrations (mol/L)	Removal (%)
HCl	0.1	48.7
	0.3	62.4
	0.5	64.9
NaOH	0.1	66.9
	0.3	87.7
	0.5	69.3
NaCl	0.1	54.5
	0.3	83.9
	0.5	59.9

3.8. Characterization of materials

Fig. 6 shows the XRD patterns of BT, the adsorbents before and after MO adsorption. From Fig. 6, the XRD pattern of BT showed the characteristic peak of montmorillonite at around 6.56°. After BT interacted with crosslinked HTCC, this peak at 6.56° was shifted to a smaller angle (6.19°), and this was accompanied by slight change in the intensity of the peak

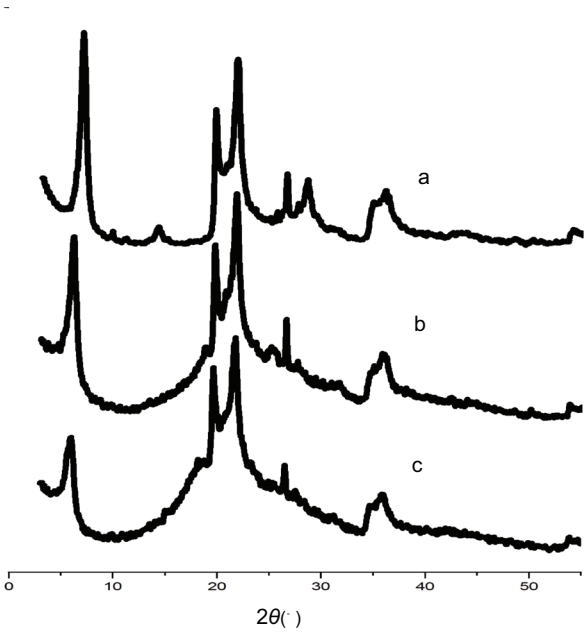

Fig. 6. XRD patterns of BT (a), crosslinked quaternized chitosan/BT composite (b) and MO loaded crosslinked quaternized chitosan/BT composite (c).

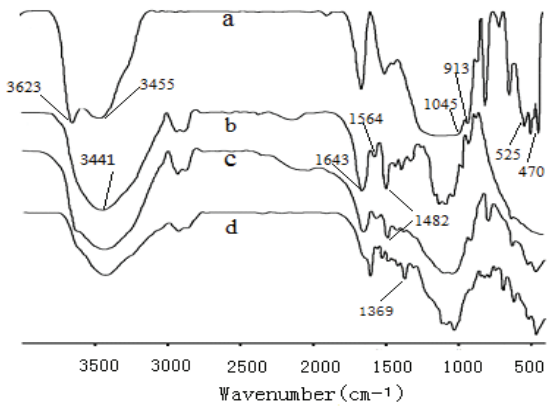

Fig. 7. FTIR patterns of BT (a), crosslinked quaternized chitosan (b), crosslinked quaternized chitosan/BT composite (c) and MO loaded crosslinked quaternized chitosan/BT composite (d).

as observed in Fig. 6. These results suggested the incorporation of crosslinked HTCC into the interlayer spacing of BT. However, after the adsorbent was loaded by MO, the intensity of the peak at 6.19° was decreased, indicating the occurrence of the reaction between MO and this composite [31].

Spectra of BT, crosslinked HTCC, and the adsorbents before and after MO adsorption were examined for functional groups that contributed to the adsorption process; the spectra are shown in Fig. 7. In the spectrum of BT, the peak at 3,623 cm^{-1} was assigned to a stretching band of the inner OH unit within the clay structure, and the peak at 3,455 cm^{-1} was related to the OH vibration of water molecules. The characteristic peaks corresponding to the phyllosilicate structure of BT appeared between 470 and 1,160 cm^{-1}. A broad peak between 1,045 and 1,160 cm^{-1} was attributed to the characteristic stretching vibration of the Si–O, and the peak at 525 cm^{-1} belonged to the angular deformation of Si–O in the tetrahedral sheet. The peaks from 915 to 794 cm^{-1} corresponded to the octahedral layers of BT.

In the spectrum of crosslinked HTCC, a broad intense peak near 3,441 cm^{-1} was attributed to the stretching vibrations of O–H and N–H groups. The peaks at 2,922 and 2,876 cm^{-1} corresponded to the C–H stretching vibrations of the alkyl group. The peaks at 1,643 and 1,564 cm^{-1} were associated to the stretching vibrations of amide and amine groups, respectively. The peak at 1,482 cm^{-1} was attributed to the methyl of the ammonium groups in HTCC [32].

After BT interacted with crosslinked HTCC, the intensities of the characteristic peaks of the amine and ammonium groups decreased as compared with those of crosslinked HTCC. The intensities of the characteristic peaks of BT changed and this was accompanied by the changes in the positions of these peaks in comparison with the spectrum of BT. These results indicated that the amine and ammonium groups in crosslinked HTCC mainly participated in the reaction with BT.

In the spectrum of the MO loaded adsorbent, the intensities of the characteristic peaks of the amine and ammonium groups decreased and even disappeared, and the positions of these peaks shifted as shown in Fig. 7. These changes indicated the amine and ammonium groups in HTCC were involved in the adsorption of MO due to the electrostatic interaction. Meanwhile, the intensities and positions of the characteristic peaks of BT were different from those of the adsorbent before MO adsorption due to the hydrogen bonds between BT and MO. The intensity of the peak near 3,441 cm^{-1} due to the stretching vibrations of O–H and N–H was decreased due to the hydrogen bonds between amine and hydroxyl groups and MO. Besides, a new peak at 1,369 cm^{-1} attributed to aromatic nitro compound was detected, indicating the presence of MO molecules on the adsorbent surface [33].

Based on the results of the adsorption experiments and FTIR analysis, the possible mechanisms for MO adsorption on the composite were obtained. These mechanisms involved the electrostatic interaction and the hydrogen bonds between this adsorbent and MO. However, the electrostatic interaction was the main mechanism of MO adsorption onto this composite.

4. Conclusion

A CHTCC/BT composite was prepared via immobilizing crosslinked quaternized chitosan into BT and used for the adsorption of MO. The MO adsorption onto the CHTCC/BT was affected by the amount of quaternized chitosan, initial pH, initial dye concentration, inorganic sodium salt, etc. Kinetic and isotherm studies showed that the pseudo-second-order model and Langmuir model could well describe the adsorption behavior. The maximum monolayer adsorption capacity of CHTCC/BT composite was 632.9 mg/g at 298 K and natural pH value. The adsorption behavior and FTIR analysis indicated that the possible adsorption mechanism of MO involved the electrostatic interaction and hydrogen bonding. Besides, the adsorbent was regenerated with 0.3 mol/L NaOH solution effectively. Therefore, the CHTCC/BT composite is expected to have a promising future for the dye-polluted water purification.

References

[1] C.I. Pearce, J.R. Lloyd, J.T. Guthrie, The removal of colour from textile wastewater using whole bacterial cells: a review, Dyes Pigm., 58 (2003) 179–196.
[2] H.J. Hou, R.H. Zhou, P. Wu, L. Wu, Removal of Congo red dye from aqueous solution with hydroxyapatite/chitosan composite, Chem. Eng. J., 211 (2012) 336–342.
[3] F. Liu, B.R. Ma, D. Zhou, L.J. Zhu, Y.Y. Fu, L.X. Xue, Positively charged loose nanofiltration membrane grafted by diallyl dimethyl ammonium chloride (DADMAC) via UV for salt and dye removal, React. Funct. Polym., 86 (2015) 191–198.
[4] R. Sanghi, B. Bhattacharya, V. Singh, Seed gum polysaccharides and their grafted co-polymers for the effective coagulation of textile dye solutions, React. Funct. Polym., 67 (2007) 495–502.
[5] A.S. Mohamed, G.E. Rehab, F.H. Mahmoud, Adsorption of brilliant green dye by polyaniline/silver nanocomposite: kinetic, equilibrium, and thermodynamic studies, Eur. Polym. J., 75 (2016) 577–590.
[6] S.M. Sayyah, A.A. Essawy, A.M. El-Nggar, Kinetic studies and grafting mechanism for methyl aniline derivatives onto chitosan: highly adsorptive copolymers for dye removal from aqueous solutions, React. Funct. Polym., 96 (2015) 50–60.
[7] C. Djilani, R. Zaghdoudi, F. Djazi, B. Bouchekima, A. Lallam, A. Modarressi, M. Rogalski, Adsorption of dyes on activated carbon prepared from apricot stones and commercial activated carbon, J. Taiwan Inst. Chem. Eng., 53 (2015) 112–121.

[8] F.A.R. Pereira, K.S. Sousa, G.R.S. Cavalcanti, M.G. Fonseca, A.G.D. Souza, A.P.M. Alves, Chitosan-montmorillonite biocomposite as an adsorbent for copper(II) cations from aqueous solutions, Int. J. Biol. Macromol., 61 (2013) 471–478.
[9] A. Giannakas, K. Grigoriadi, A. Leontiou, N.M. Barkoula, A. Ladavos, Preparation, characterization, mechanical and barrier properties investigation of chitosan-clay nanocomposites, Carbohydr. Polym., 108 (2014) 103–111.
[10] S.F. Wang, L. Shen, Y.J. Tong, L. Chen, I.Y. Phang, P.Q. Lim, T.X. Liu, Biopolymer chitosan/montmorillonite nanocomposites: preparation and characterization, Polym. Degrad. Stab., 90 (2015) 123–131.
[11] V.A. Spinelli, M.C.M. Laranjeira, V.T. Fávere, Preparation and characterization of quaternary chitosan salt: adsorption equilibrium of chromium(VI) ion, React. Funct. Polym., 61 (2004) 347–352.
[12] R. Li, P. Li, J. Cai, S.J. Xiao, H. Yang, A.M. Li, Efficient adsorption of both methyl orange and chromium from their aqueous mixtures using a quaternary ammonium salt modified chitosan magnetic composite adsorbent, Chemosphere, 154 (2016) 310–318.
[13] X.Y. Li, Y. Han, Y.Z. Ling, X.Y. Wang, R.C. Sun, Assembly of layered silicate loaded quaternized chitosan/reduced graphene oxide composites as efficient absorbents for double-stranded DNA, ACS Sustain. Chem. Eng., 3 (2015) 1846–1852.
[14] J.H. Cai, W.J. Ye, X.Y. Wang, W.S. Lin, Q.X. Lin, Q. Zhang, F.C.Y. Wu, Preparation of copper-chelate quaternized carboxymethyl chitosan/organic rectorite nanocomposites for algae inhibition, Carbohydr. Polym., 151 (2016) 130–134.
[15] M.H. Lai, P. Liu, H.B. Lin, Y.Q. Luo, H.B. Li, X.Y. Wang, R.C. Sun, Interaction between chitosan-based clay nanocomposites and cellulose in a chemical pulp suspension, Carbohydr. Polym., 137 (2016) 375–381.
[16] J.W. Luo, G.C. Han, M.J. Xie, Z.R. Cai, X.Y. Wang, Quaternized chitosan/montmorillonite nanocomposite resin and its adsorption behavior, Iran. Polym. J., 24 (2015) 531–539.
[17] R.H. Huang, B.C. Yang, D.S. Zheng, B. Wang, Preparation and characterization of a quaternized chitosan, J. Mater. Sci., 47 (2012) 845–851.
[18] P. Monvisade, P. Siriphannon, Chitosan intercalated montmorillonite: preparation, characterization and cationic dye adsorption, Appl. Clay Sci., 42 (2009) 427–431.
[19] H.Y. Zhu, R. Jiang, Y.Q. Fu, J.H. Jiang, L. Xiao, G.M. Zeng, Preparation, characterization and dye adsorption properties of γ-Fe_2O_3/SiO_2/chitosan composite, Appl. Surf. Sci., 258 (2011) 1337–1344.
[20] E.H. Mekatel, S. Amokrane, A. Aid, D. Nibou, M. Trari, Adsorption of methyl orange on nanoparticles of a synthetic zeolite NaA/CuO, C.R. Chim., 18 (2015) 336–344.
[21] Z.H. Wang, B. Xiang, R.M. Cheng, Y.J. Li, Behaviors and mechanism of acid dyes sorption onto diethylenetriamine-modified native and enzymatic hydrolysis starch, J. Hazard. Mater., 183 (2010) 224–232.
[22] Z. Li, R. Beachner, Z. McManama, H.L. Hong, Sorption of arsenic by surfactant-modified zeolite and kaolinite, Microporous Mesoporous Mater., 105 (2007) 291–297.
[23] R. Lafi, A. Hafiane, Removal of methyl orange (MO) from aqueous solution using cationic surfactants modified coffee waste (MCWs), J. Taiwan Inst. Chem. Eng., 58 (2016) 424–433.
[24] S. Largergren, Zur theorie der sogenannten adsorption geloster stoffe, K. Sven. Vetensk.akad. Handl., 24 (1898) 1–39.
[25] Y.S. Ho, G. McKay, Pseudo-second order model for sorption processes, Process. Biochem., 34 (1999) 451–465.
[26] L.F. Zhang, X. Liu, W. Xia, W.Q. Zhang, Preparation and characterization of chitosan-zirconium(IV) composite for adsorption of vanadium(V), Int. J. Biol. Macromol., 64 (2014) 155–161.
[27] Y.A. El-Reash, M. Otto, I.M. Kenawy, A.M. Ouf, Adsorption of Cr(VI) and As(V) ions by modified magnetic chitosan chelating resin, Int. J. Biol. Macromol., 49 (2011) 513–522.
[28] H.H.D. Santo, C.A. Demarchi, C.A. Rodrigues, J.M. Greneche, N. Nedelko, A. Slawska-Waniewska, Adsorption of As(III) on chitosan-Fe-crosslinked complex, Chemosphere, 82 (2011) 278–283.
[29] D.J. Wan, H.J. Liu, R.P. Liu, J.H. Qu, S.S. Li, J. Zhang, Adsorption of nitrate and nitrite from aqueous solution onto calcined (Mg–Al) hydrotalcite of different Mg/Al ratio, Chem. Eng. J., 195 (2012) 241–247.
[30] M.M. Dubinin, L.V. Radushkevich, Proceedings of the academy of sciences of the USSR, Phys. Chem., 55 (1947) 327–329.
[31] L.J. Zhang, P. Hu, J. Wang, R.H. Huang, Crosslinked quaternized chitosan/bentonite composite for the removal of Amino black 10B from aqueous solutions, Int. J. Biol. Macromol., 93 (2016) 217–225.
[32] X.Y. Li, B. Liu, W.J. Ye, X.Y. Wang, R.C. Sun, Effect of rectorite on the synthesis of AgNP and its catalytic activity, Mater. Chem. Phys., 151 (2015) 301–307.
[33] M. Auta, B.H. Hameed, Chitosan-clay composite as highly effective and low-cost adsorbent for batch and fixed-bed adsorption of methylene blue, Chem. Eng. J., 237 (2014) 352–361.

Supplementary materials

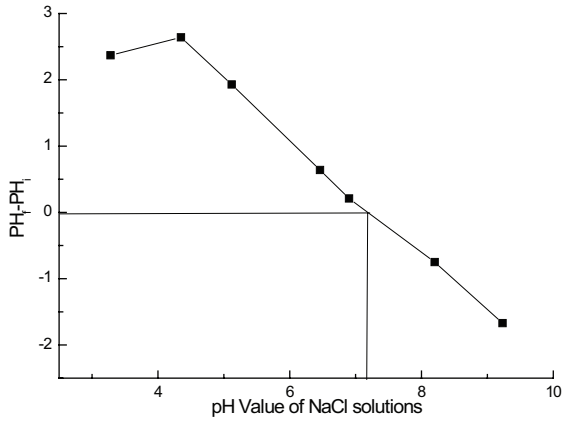

Fig. S1. Determination of pH_{pzc} of CHTCC/BT composite.

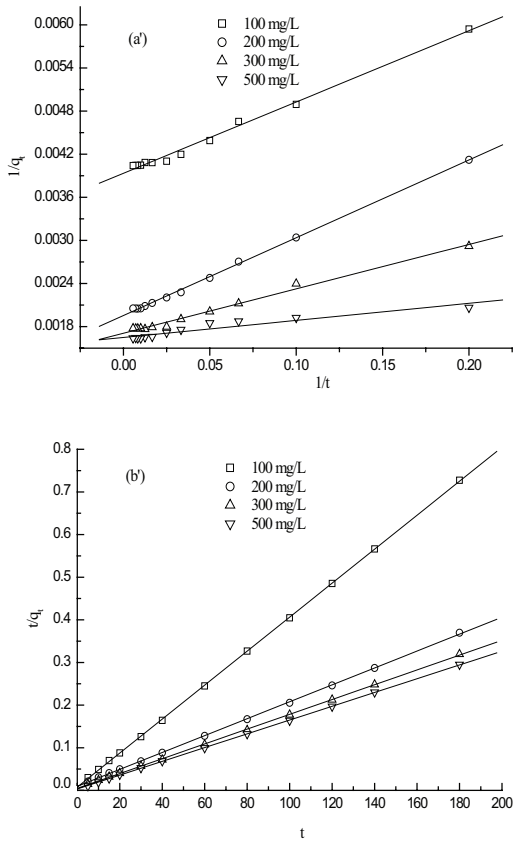

Fig. S2. Plots of pseudo-first-order model (a′) and pseudo-second-order model (b′).

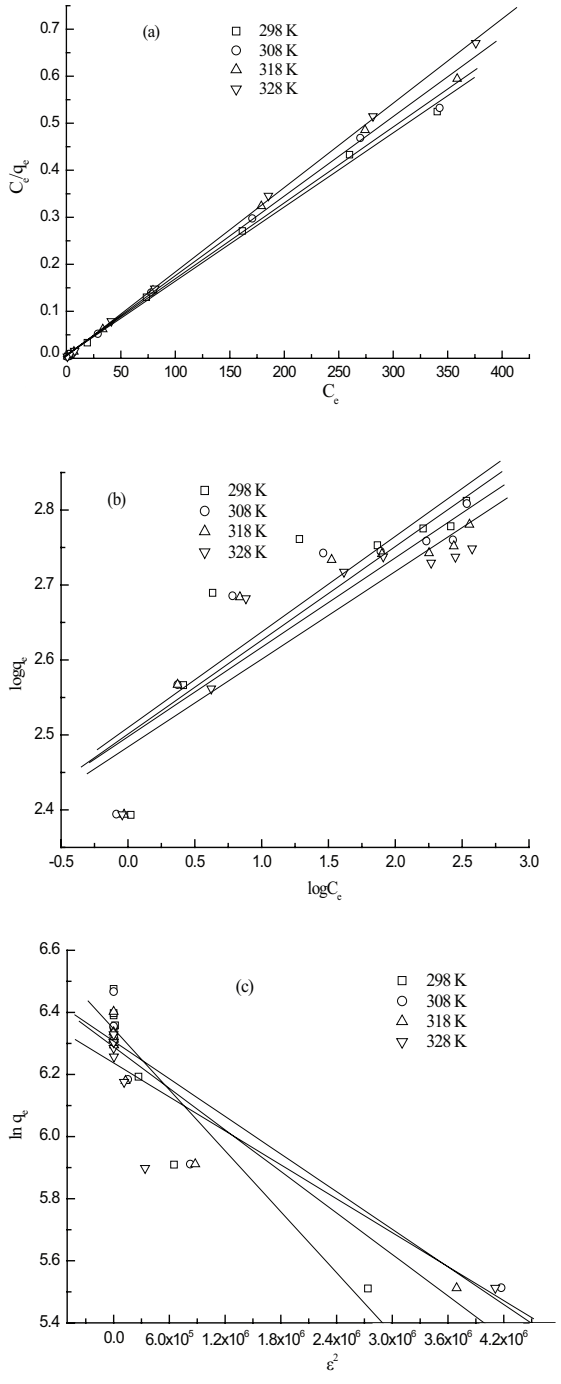

Fig. S3. Plots of the Langmuir (a′), Freundlich (b′) and D–R (c′) adsorption isotherms.